Journal of the Korean Physical Society, Vol. 73, No. 1, July 2018, pp. 90∼94

Investigation of a Rayleigh-Like Instability During the Solid-State Dewetting of Single-Crystal Nickel and Palladium Films

Jaehoon Jeong, Kyeonggon Choi and Jongpil Ye*
Department of Materials Science and Engineering, Inha University, Incheon 22212, Korea

(Received 23 February 2018, in final form 14 March 2018)

We report the results of an investigation of the Rayleigh-like instability during the solid-state dewetting of stripe patches patterned from 30-nm-thick single-crystal Ni(100) and Pd(100) films. The stability of the dewetting lines is shown to be highly anisotropic, leading to a strong dependence of the interspacing of the dewetted particles on the crystallographic orientations of the patches. The dewetting lines are most stable against the Rayleigh-like instability in the <011> or the <001> direction, resulting in maximum interparticle spacing. The stability of the <011> and that of the <001> lines are observed to increase under the condition in which oxygen adsorption on the film's surface decreases and increases, respectively. The mean interspacing of the particles can be controlled by using artificial perturbations along the patch edges, and its dispersion is significantly narrowed in the direction in which the spontaneous wavelength is comparable to or greater than the characteristic length scale of a given artificial perturbation.

PACS numbers: 61.30.Hn, 68.55.−a, 42.15.−i, 68.55.J−
Keywords: Dewetting, Nickel, Palladium, Single crystal, Rayleigh-like instability
DOI: 10.3938/jkps.73.90

I. INTRODUCTION

Thin solid films are usually thermodynamically metastable and dewet into an array of isolated islands when heated to high temperatures. This morphological evolution often begins with the formation of holes that reach the substrate's surface [1]. A capillary force at the three-phase boundary of the film, substrate, and ambient drives the surface diffusion of the film's material to the top film's surface, causing the hole edges to retract and thicken [2,3]. During the later stage of dewetting, the thickened edges, the so called rims, are subject to a series of instabilities that include the corner-induced instability [4], pinch-off [5,6], and the fingering instability [7]; such instabilities lead to the formation of separate cylindrical lines. As the surface energy of these cylindrical lines can be further reduced by amplifying the periodical surface perturbation, these lines finally decay to form an array of islands [8]. The instability driving this type of morphological evolution is called a Rayleigh-like instability (see the scheme Fig. 1) [9]. Because of the stochastic nature of the hole nucleation and dewetting processes [2, 10, 11], the dewetted particle arrays formed via the Rayleigh-like instability show a random distribution and large dispersions of size and interspacing.

Dewetted metal particles have been widely used in plasmonics [12–14]. However, a lack of precise control of their size and position still limits their application in commercial devices. In recent years, thin-film dewetting has been utilized to produce an ordered array of metal nanoparticles by pre-patterning continuous films into stripes or ring patches before subjecting them to the dewetting process [15–18]. The pre-patterning of the films geometrically constrains edge retraction and suppresses hole nucleation inside the patches, thereby narrowing the dispersions of the sizes and the positions of the particles formed via a Rayleigh-like instability. The sizes and the positions of the particles were found to depend strongly on the patch's geometry and the annealing condition. Hence, if precise control over the size and the position of the dewetted particles is to be obtained, the dewetting processes and the designs of the patch's geometries should be optimized by considering the mechanisms for the formation of the particles via a Rayleigh-like instability.

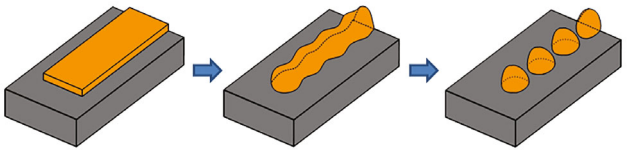

Fig. 1. (Color online) Schematic illustration of the formation of an array of particles via a Rayleigh-like instability during the dewetting of a thin film [9].

*E-mail: jpye@inha.ac.kr

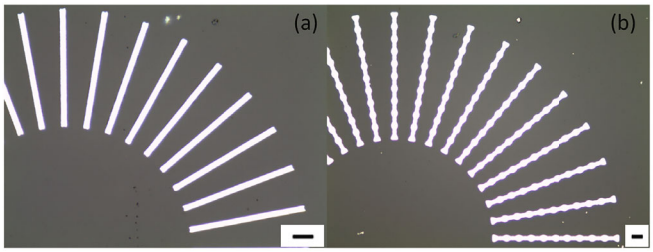

Fig. 2. (Color online) OM images of polar arrays of as-patterned (a) straight and (b) perturbed stripe patches. The scale bars represent 10 μm.

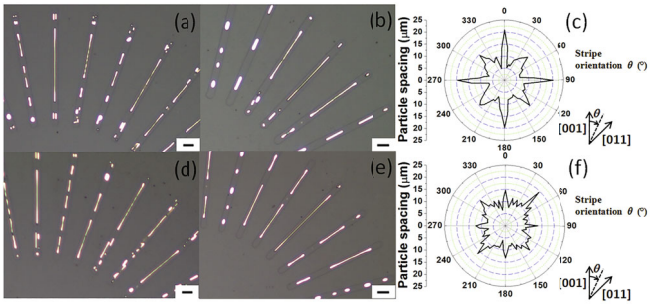

Fig. 3. (Color online) Dewetting results of stripe patches patterned from 30-nm-thick Ni(100) films. The samples were annealed at 900 °C for 30 min in (a) - (c) 5 sccm and (d) - (f) 100 sccm of hydrogen and 200 sccm of argon. (a), (b), (d), and (e) are OM images of arrays of dewetted particles aligned along various directions. The scale bars represent 5 μm. (c) and (f) are the polar plots of particle interspacing as a function of the angle between each edge orientation and the [001] direction. The crystallographic directions are indicated at the middle and lower right side of the figure.

In the case of single-crystal films, the dewetting of patches is crystallographically constrained. This additional constraint can further improve the control of the size and the position of the dewetted particles. The improvement has been shown to originate from the effect of the surface-energy anisotropy of the film's material on the Rayleigh-like instability [9,17,18]. Because the surface-energy anisotropy strongly depends on the film's material and the annealing conditions, a careful investigation of their effect on the Rayleigh-like instability is required for the application of the phenomenon to obtain precise control over dewetting morphologies for a wide range of materials. Herein, we present the results of an investigation of the Rayleigh-like instability during the solid-state dewetting of single-crystal nickel and palladium films. By analyzing the interspacings of the particles formed by the dewetting of the stripe patches aligned along various directions, we show that the film's material and the annealing ambient have significant effects on the anisotropic Rayleigh-like instability. We also show that the size and the position of the dewetted particles can be further controlled by introducing periodic perturbations into the edges of the stripe patches. The results of this investigation will guide design of the patterning and the annealing processes for obtaining well-controlled arrays by using the solid-state dewetting of single-crystal films.

II. EXPERIMENTAL DETAILS

Thirty-nm-thick single-crystal Ni and Pd films were epitaxially grown on epi-polished single crystal (100)-oriented MgO substrates (Crystec, Germany) by using electron beam evaporation. The MgO substrates were pre-heated prior to the deposition process for desorbing the gas molecules adsorbed on them. The deposition rate was measured to be 0.5 Å/s by using a quartz crystal sensor. The chamber pressure was initially at low 10^{-6} Torr and was increased to and maintained at mid 10^{-6} Torr. The deposition temperature was 320 °C. The as-deposited Ni and Pd films were patterned by using photolithography into straight and perturbed stripe patches aligned along various directions. This was followed by acid-base wet or dry etching (See Fig. 2). The recipes for the etching processes have been reported elsewhere [17,18]. The patterned Ni and Pd films were annealed in a quartz tube furnace at 900 °C in different atmospheres of hydrogen and argon. The temperature was calibrated using a K-type thermoprobe, and the rate of gas flow was measured using mass-flow controllers. The dewetting morphologies were observed and analyzed using an optical microscope (OM; BX41M, Olympus).

III. RESULTS AND DISCUSSION

Figure 3 shows the dewetting results for the straight stripe patches patterned from 30-nm-thick Ni(100) films. As seen in the OM images, stripe patches dewet into an array of lines and particles with a mean interspacing that strongly depends on the crystallographic alignment of the patches. The lines aligned along the <001> and the <011> directions show greater stability against the Rayleigh-like instability. The particle interspacing also strongly depends on the flow rate of hydrogen. The interspacing polar plots in Figs. 3(c) and 3(f) clearly show the effects on the particle interspacing of the crystallographic alignment of patches and the hydrogen flow rate. In the case of the patches annealed in 100 sccm (standard cubic centimeters per minute) of hydrogen and 200 sccm of argon (see Fig. 3(f)), the polar plots show local maxima of comparable values along two inequivalent directions (<001> and <011>). When the flow rate of hydrogen is decreased to 5 sccm, the particle interspacing along the <001> directions increases by approximately 33%, whereas it decreases by approximately 10% along the <011> directions, as shown in Fig. 3(c). This change in the polar plot can be understood in terms of the effect of oxygen adsorption on the surface-energy anisotropy of

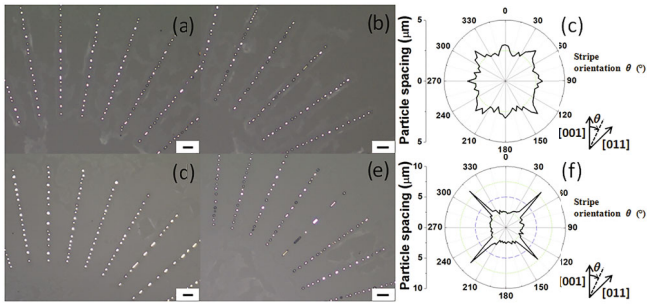

Fig. 4. (Color online) Dewetting results of stripe patches patterned from 30-nm-thick Pd(100) films. The samples were annealed at 900 °C for 30 min in (a) - (c) 5 sccm and (d) - (f) 100 sccm of hydrogen and 200 sccm of argon. (a), (b), (d), and (e) are OM images of arrays of dewetted particles aligned along various directions. The scale bars represent 5 μm. (c) and (f) are the polar plots of particle interspacing as a function of the angle between each edge orientation and the [001] direction. The crystallographic directions are indicated at the middle and lower right side of the figure.

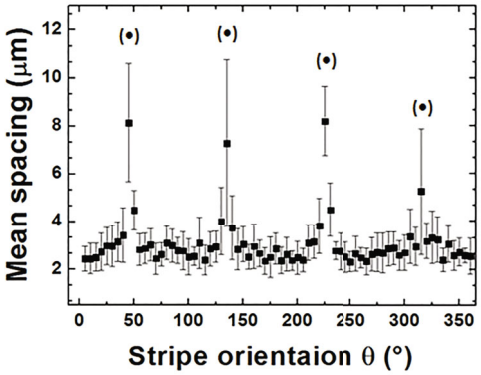

Fig. 5. Mean and dispersion of the interspacing of particles formed by the dewetting of straight stripe patches shown in Figs. 4(d) and 4(e).

nickel and the stability against the Rayleigh-like instability [17].

Faceting along the surface of lines is well known to be able to stabilize the line morphologies against the Rayleigh-like instability [8]. In the case of clean Ni surfaces, faceting occurs at low energy and low index orientations such as {111} and {100}. Hence, the Ni lines remain stable when aligned along the directions along which the rim surfaces are crystallographically constrained for exposing these low index facets without being perturbed along their long axes. These directions correspond to the <011> or the <001> directions in Ni(100) films [18]. As the flow rate of hydrogen is decreased, the level of oxygen adsorption on the evolving film's surface will increases, thereby changing the surface-energy anisotropy of nickel in such a way that high-index {hk0} facets appear clearly while the prominence of {111} facets is decreased. Given that {hk0} facets can be exposed along the surface of lines aligned along the <001> directions, the substantial increase in particle spacing along the <001> directions is seen to arise from the formation of high-index facets under a relatively low flow rate of hydrogen. Of note is that infinite lines were used in the model, suggesting the complete stability of the faceted lines against the Rayleigh-like instability. Because the stripe patches used in our investigation are finite, spheroidization and pearling occur at the ends of the patches, resulting in a finite interparticle spacing.

Figure 4 shows the results of dewetting of 30-nm-thick Pd(100) straight stripe patches. These results are qualitatively consistent with those of the Ni stripe patches in terms of the effects of the crystallographic alignments of the patches and the hydrogen flow rate on the interspacing of the particles formed via the Rayleigh-like instability. The followings are commonly observed in the dewetting results of Ni and Pd patches. The local maxima in the interspacing polar plot appear in the <001> or the <011> directions and the maxima in the <001> directions become prominent as the hydrogen flow rate decreases. However, in the case of Pd(100) patches, the local maxima along the <011> directions are measured to be more prominent than those along the <001> directions for the two flow rates of hydrogen. Furthermore, as seen in comparing the polar plots of Figs. 3 and 4, the local maxima along the <011> directions are observed to be more prominent in Pd films than in Ni films for a given flow rate of hydrogen.

This difference is consistent with the results from recent studies [17,19] suggesting that the difference in the dewetting behaviors of single-crystal Ni and Pd films annealed in the same ambient arises owing to the difference in the levels of oxygen adsorption on the surfaces of the two metals. This explanation was based on the driving force for palladium oxidation being smaller than that for nickel oxidation. Because of this difference, the extent of oxygen adsorption will be lower on Pd surfaces than on Ni surfaces, leading to the formation of more prominent {111} facets, which are the planes of minimum surface energy in the case of clean surfaces of face-centered-cubic metals with no impurity adsorption. The lower level of oxygen adsorption on Pd surfaces is seen to affect critically the finding that the interparticle spacing along the <011> directions is significantly greater than that along other directions in Pd films compared to the case of Ni.

As shown in Figs. 3 and 4, the dewetted particles show characteristic interspacings that strongly depend on the in-plane orientations of the stripe patches; however, substantial interspacing dispersions are seen in the <011> or the <001> directions. For example, this can be clearly seen in Fig. 5, which shows maximum dispersion along the <011> directions of Pd annealed in 100 sccm of hydrogen and 200 sccm of argon (see the data indicated by filled circles in a parentheses). This large dispersion is associated with the greatest line stability against the

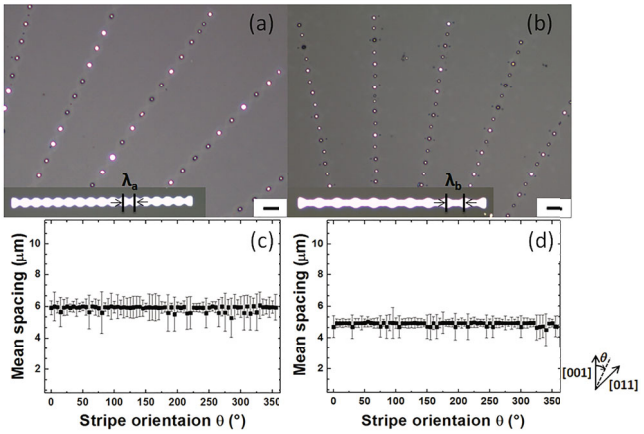

Fig. 6. (Color online) Effect of an artificial perturbation on the interspacing of particles formed via the Rayleigh-like instability. (a) and (b) are OM images of particles formed by dewetting two types of Pd(100) patches with different artificial perturbations. The initial shape of the pre-perturbed patch is shown in the inset (λ_a = 6 μm, λ_b = 10 μm). The scale bars represent 5 μm. (c) and (d) are the plots of the interspacing of particles formed by the dewetting of patches with the artificial perturbation of (a) and (b). The samples were annealed at 900 °C in 100 sccm of hydrogen and 200 sccm of argon for 30 min. The crystallographic directions are indicated in the lower right corner.

Rayleigh-like instability along these directions. In other directions, the edges of the stripe patches are spontaneously and periodically perturbed to expose low-index facets such as {111} and {100}, thereby directing the Rayleigh-like instability to form an array of particles with a characteristic interspacing of relatively low dispersion. The absence of this periodic perturbation along the <011> or the <001> directions results in a large dispersion of the particle interspacing. The large dispersion of the interspacing of particles along these directions can be substantially reduced by introducing an artificial perturbation along the edges of the patches in the prepatterning process. Figures 6(a) and 6(b) show the arrays of particles formed as a result of dewetting of two types of Pd(100) patches with different artificial perturbations. These patches were also annealed in 100 sccm of hydrogen and 200 sccm of argon. The periods of the artificial perturbations are indicated in the insets of the figures. The dispersion of the particle interspacing in the <011> directions was observed to be significantly narrowed by the artificial perturbation, as seen in comparing Fig. 5 to Figs. 6(c) and 6(d). The nearly-orientation-independent particle interspacings shown in Figs. 6(c) and 6(d) are approximately 6 μm and 5 μm, which are close to the period and the half-period of the artificial perturbation, respectively, suggesting that the characteristic wavelength of the Rayleigh-like instability is dictated by the artificial perturbation.

Neither artificial perturbations, however, leads to a notable decrease in the dispersion of the particle interspacing along most directions other than the <011> directions. As shown in Fig. 5, the average interspacing of particles formed from straight stripe patches is relatively small along these directions. As the characteristic length scale (period or half-period) of the artificial perturbations is considerably greater than the spontaneous wavelength along these directions, both the faceting-induced spontaneous perturbation and artificial perturbation can simultaneously affect the Rayleigh-like instability, resulting in the formation of particles without a significant decrease in the dispersion of the particle interspacing. This suggests that the characteristic length scale of an artificial perturbation should be designed to be smaller than or comparable to the wavelength of the spontaneous perturbation in order to narrow significantly the distribution of the particle interspacing.

IV. CONCLUSION

In conclusion, we present the results obtained from an investigation of the Rayleigh-like instability during solid-state dewetting of single-crystal Ni(100) and Pd(100) films. By analyzing the interspacing of particles formed by the dewetting of stripe patches aligned along different directions, we show that the stability of lines against the Rayleigh-like instability strongly depends on the patch orientation, film's materials, and hydrogen flow rate. The stability of the lines is found to be greater along the <011> and the <001> directions compared to the other directions; the <011> and the <001> lines exhibit the greatest stability under the conditions of high and low levels of oxygen adsorption, respectively. The particle interspacing is controllable with artificial perturbations, and its dispersion is significantly reduced when the characteristic length scale of the artificial perturbation is shorter than or comparable to the spontaneous wavelength. We expect that this work will lead to better quantitative predictions of the morphological characteristics of particle arrays formed via the Rayleigh-like instability for a wide range of materials.

ACKNOWLEDGMENTS

This work was supported by an Inha University research grant (INHA-55768).

REFERENCES

[1] C. V. Thompson, Annual Rev. Mater. Res. **42**, 399 (2012).
[2] E. Jiran and C. V. Thompson, J. Electron. Mater. **19**, 1153 (1990).

[3] E. Jiran and C. V. Thompson, Thin Solid Films **208**, 23 (1992).
[4] J. P. Ye and C. V. Thompson, Appl. Phys. Lett. **97**, 071904 (2010).
[5] H. Wong, P. W. Voorhees, M. J. Miksis and S. H. Davis, Acta Mater. **48**, 1719 (2000).
[6] J. Ye and C. V. Thompson, Phys. Rev. B **82**, 193408 (2010).
[7] W. Kan and H. Wong, J. Appl. Phys. **97**, 043515 (2005).
[8] F. A. Nichols and W. W. Mullins, Trans. Am. Instit. Mining **233**, 1840 (1965).
[9] G. H. Kim and C. V. Thompson, Acta Mater. **84**, 190 (2015).
[10] J. Ye, Appl. Phys. Exp. **7**, 085601 (2014).
[11] R. Seemann, S. Herminghaus and K. Jacobs, J. Phys. -Conden. Matter **13**, 4925 (2001).
[12] H. A. Atwater and A. Polman, Nat. Mater. **9**, 205 (2010).
[13] G. Maidecchi, G. Gonella, R. P. Zaccaria, R. Moroni, L. Anghinolfi, A. Giglia, S. Nannarone, L. Mattera, H-L. Dai, M. Canepa and F. Bisio, ACS Nano **7**, 5834 (2013).
[14] R. W. Yu, P. Mazumder, N. F. Borrelli, A. Carrilero, D. S. Ghosh, R. A. Maniyara, D. Baker, F. J. Garcia de Abajo and V. Pruneri, ACS Photo. **3**, 1194 (2016).
[15] J. D. Fowlkes, L. Kondic, J. Diez, Y. Wu and P. D. Rack, Nano Lett. **11**, 2478 (2011).
[16] J. Lian, L. Wang, X. Sun, Q. Yu and R. C. Ewing, Nano Lett. **6**, 1047 (2006).
[17] J. Ye, Sci. Rep. **5**, 9823 (2015).
[18] J. Ye and C. V. Thompson, Adv. Mater. **23**, 1567 (2011).
[19] J. Ye, J. Vac. Sci. Tech. A **33**, 060601 (2015).